

Electronic properties of corrugated graphene.



F. Guinea

A. Castro-Neto (Boston U.), N. M. R. Peres (U. Minho, Portugal), E. V. Castro, J. dos Santos (Porto), J. Nilsson (Boston U.), A. Morpurgo (Delft), M. I. Katsnelson (Nijmegen), D. Huertas-Hernando (Trondheim, Norway), D. P. Arovas, M. M. Fogler (U. C. San Diego), J. González, F. G., G. León, M. P. López-Sancho, T. Stauber, J. A. Vergés, M. A. H. Vozmediano, B Wunsch (CSIC, Madrid), A. K. Geim, K. S. Novoselov (U. Manchester), A. Lanzara (U. C. Berkeley), M. Hentschel (Dresden), E. Prada, P. San-José (Karlsruhe, Lancaster), J. L. Mañes (U. País Vasco, Spain), F. Sols (U. Complutense, Madrid), E. Louis (U. Alicante, Spain), A. L. Vázquez de Parga, R. Miranda (U. Autónoma, Madrid), B. Horovitz (Beersheva), P. Le Doussal (ENS, Paris), A. K. Savchenko (Exeter).

KITP Conference on
New Directions in Low-
Dimensional Electron
Systems. Feb. 23-27,
2009

Outline

- Disorder and the Dirac equation
- Lattice strains, topological defects and curvature
- Effective magnetic fields
- Random gauge fields
- Zero modes, interaction effects
- Strains in suspended samples
- Mesoscopic effective magnetic fields

Midgap states and charge instabilities in corrugated graphene, F. G., M. I. Katsnelson, and M. A. H. Vozmediano, Phys. Rev. B **77**, 075422 (2008)

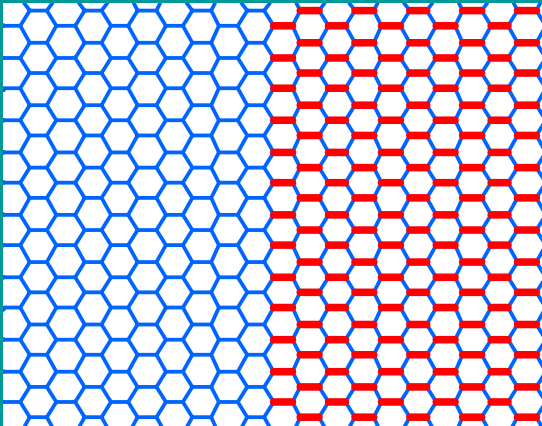
Gauge field induced by ripples in graphene, F. G., B. Horovitz and P. Le Doussal, Phys. Rev. B **77**, 205421 (2008)

Pseudomagnetic fields and ballistic transport in suspended graphene sheets, M. M. Fogler, F. G., and M. I. Katsnelson, Phys. Rev. Lett. **101**, 226804 (2008)

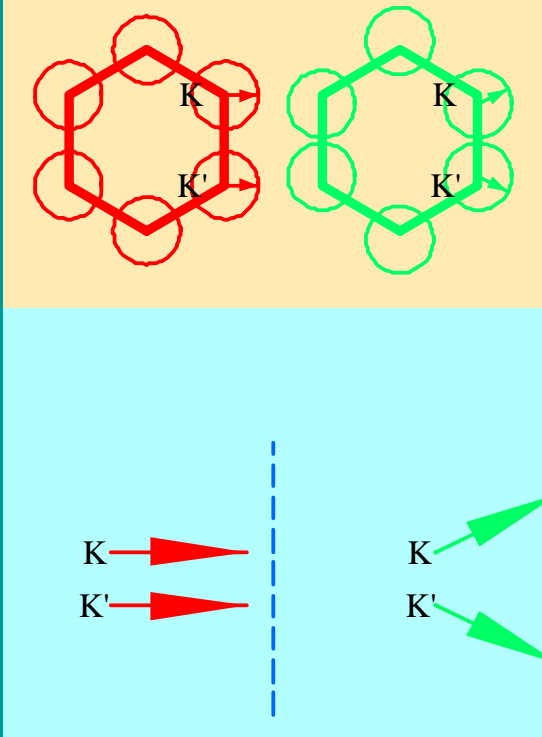
The electronic properties of graphene, A. H. Castro Neto, F. G., N. M. R. Peres,..A. K. Geim, K. S. Novoselov, Rev. Mod. Phys. **81**, 109 (2009)

M. A. H. Vozmediano, M. I. Katsnelson, F. G., in preparation, A. K. Geim, M. I. Katsnelson, F. G., in preparation

Effective gauge fields



$$H \equiv \begin{pmatrix} 0 & t_1 e^{i\vec{k}_1 \cdot \vec{a}_1} + t_2 e^{i\vec{k}_2 \cdot \vec{a}_2} + t_3 e^{i\vec{k}_3 \cdot \vec{a}_3} \\ t_1 e^{-i\vec{k}_1 \cdot \vec{a}_1} + t_2 e^{-i\vec{k}_2 \cdot \vec{a}_2} + t_3 e^{-i\vec{k}_3 \cdot \vec{a}_3} & 0 \end{pmatrix} \approx \begin{pmatrix} 0 & \frac{3\bar{t}a}{2}(k_x + ik_y) + \Delta t \\ \frac{3\bar{t}a}{2}(k_x + ik_y) + \Delta t & 0 \end{pmatrix}$$



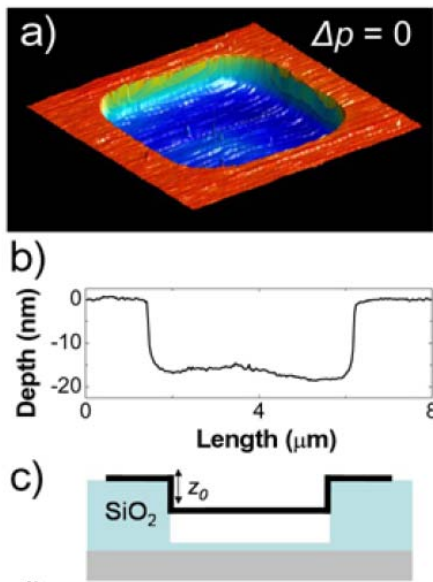
A modulation of the hoppings leads to a term which modifies the momentum: an effective gauge field.

The induced “magnetic” fields have opposite sign at the two corners of the Brillouin Zone.

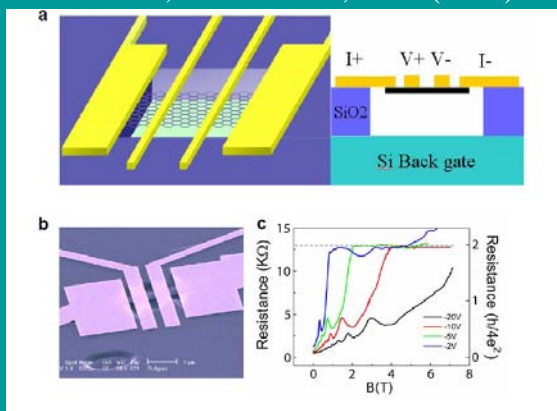
These terms are forbidden by symmetry in clean graphene.

Suspended graphene. Graphene membranes

3



J. S. Bunch, S. S. Verbridge, J. S. Alden, A. M. van der Zande, J. M. Parpia, H. G. Craighead, and P. L. McEuen, *Nano Lett.* **8**, 2458 (2008)



X. Du, I. Skachko, A. Barker, E. Y. Andrei, *Nature Nanotechnology* **3**, 491 (2008)

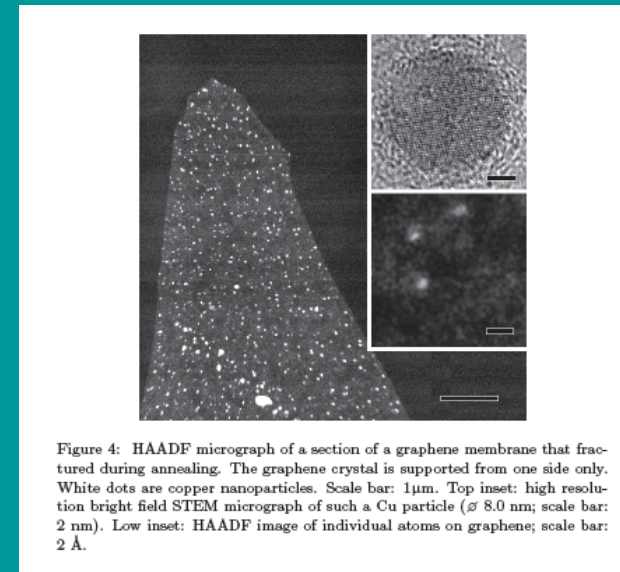


Figure 4: HAADF micrograph of a section of a graphene membrane that fractured during annealing. The graphene crystal is supported from one side only. White dots are copper nanoparticles. Scale bar: $1\mu\text{m}$. Top inset: high resolution bright field STEM micrograph of such a Cu particle ($\varnothing 8.0\text{ nm}$; scale bar: 2 nm). Low inset: HAADF image of individual atoms on graphene; scale bar: 2 \AA .

T. J. Booth, P. Blake, R. R. Nair, D. Jiang, E. W. Hill, U. Bangert, A. Bleloch, M. Gass, K. S. Novoselov, M. I. Katsnelson, and A. K. Geim, *Nano Lett.* **8**, 2442 (2008)

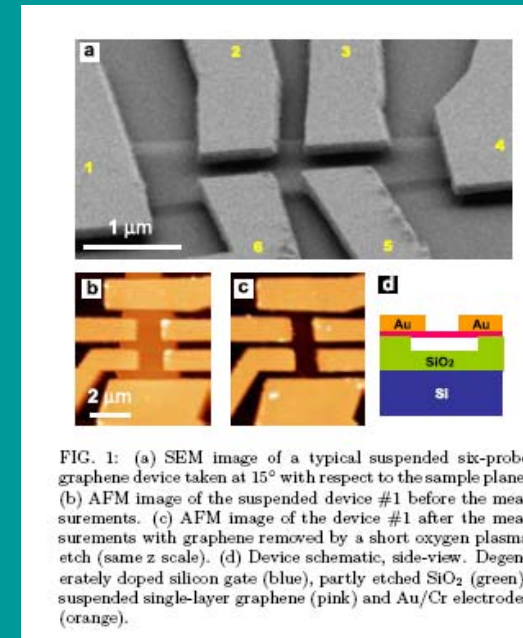
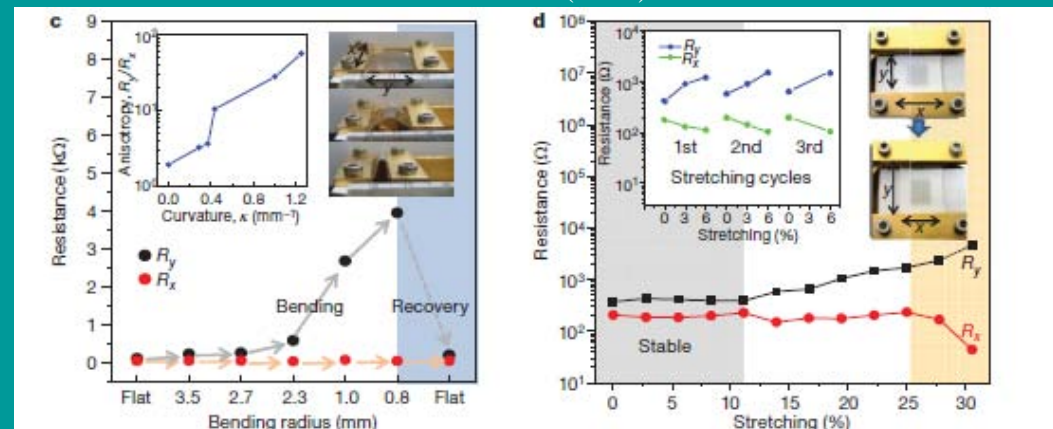


FIG. 1: (a) SEM image of a typical suspended six-probe graphene device taken at 15° with respect to the sample plane. (b) AFM image of the suspended device #1 before the measurements. (c) AFM image of the device #1 after the measurements with graphene removed by a short oxygen plasma etch (same z scale). (d) Device schematic, side-view. Degenerately doped silicon gate (blue), partly etched SiO_2 (green), suspended single-layer graphene (pink) and Au/Cr electrodes (orange).

K. I. Bolotin, K. J. Sikes, Z. Jiang, G. Fudenberg, J. Hone, P. Kim, and H. L. Stormer, *Solid St. Commun.* **146**, 351 (2008)



K. S. Kim, Y. Zhao, H. Jang, S. Y. Lee, J. M. Kim, K. S. Kim, J. H. Ahn, P. Kim, J.-Y. Choi, B. H. Hong, *Nature* **457**, 706 (2008)

Suspended graphene. Graphene membranes

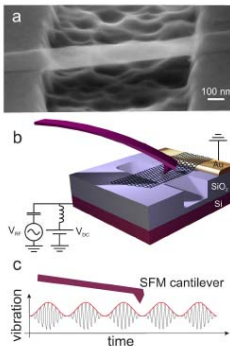


Figure 1 Device and experimental setup. **a**, A scanning electron microscope image of a suspended graphene resonator. **b**, Schematic of the resonator together with the SFM cantilever. **c** Motion of the suspended graphene sheet as a function of time. A high-frequency term at f_{RF} is matched to the resonance frequency of the graphene, and the resulting oscillation is modulated at f_{mod} .

D. García-Sánchez, A. M. van der Zande, A. San Paulo, B. Lassagne, P. L. McEuen, A. Bachtold, *Nano Lett.* **8**, 1399 (2008)

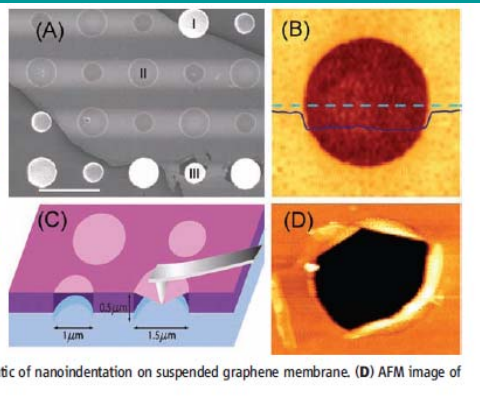


Fig. 1. Images of suspended graphene membranes. **(A)** Scanning electron micrograph of a large graphene flake spanning an array of circular holes $1\ \mu\text{m}$ and $1.5\ \mu\text{m}$ in diameter. Area I shows a hole partially covered by graphene, area II is fully covered, and area III is fractured from indentation. Scale bar, $3\ \mu\text{m}$. **(B)** Noncontact mode AFM image of one membrane, $1.5\ \mu\text{m}$ in diameter. The solid blue line is a height profile along the dashed line. The step height at the edge of the membrane is about $2.5\ \text{nm}$. **(C)** Schematic of nanoindentation on suspended graphene membrane. **(D)** AFM image of a fractured membrane.

C. Lee, X. Wei, J. W. Kysar, J. Hone, *Science* **321**, 385 (2008)

Graphene Ripples Lau Group University of California, Riverside

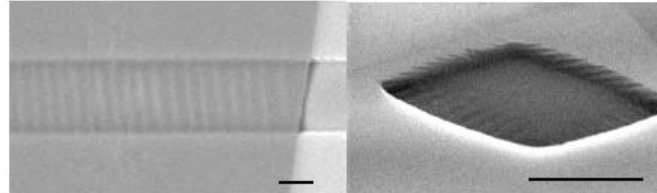
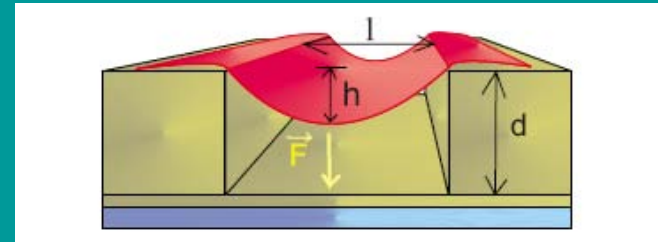


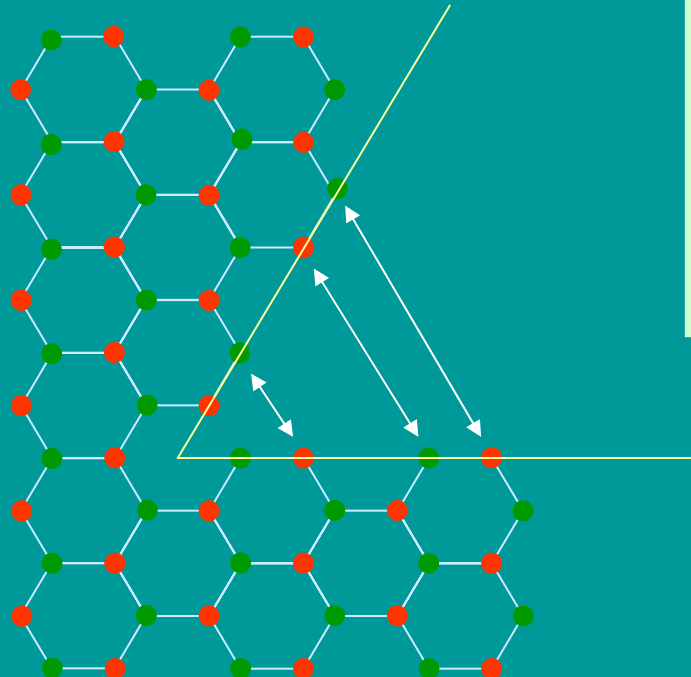
Fig. 1. SEM images of 1D and 2D ripples on suspended graphene membranes, **(a)** over a trench **(b)** over a square opening on the substrate. Scale bars: $1\ \mu\text{m}$.



M. M. Fogler, F. G., M. I. Katsnelson, *Phys. Rev. Lett.* **101**, 226804 (2008)

Lattice frustration as a gauge potential.

J. González, F. G. and M. A. H. Vozmediano, Phys. Rev. Lett. **69**, 172 (1992)



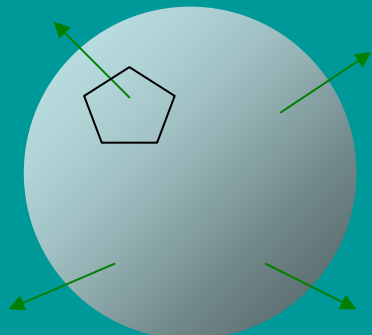
- A fivefold ring defines a disclination.
- The sublattices are interchanged.
- The Fermi points are also interchanged.
- These transformations can be achieved by means of a gauge potential.

$$i\vec{\nabla} \rightarrow i\vec{\nabla} - \vec{A} \begin{pmatrix} 0 & 1 \\ 1 & 0 \end{pmatrix}$$

$$\Phi = \int \vec{A} d\vec{l}$$

The flux Φ is determined by the total rotation induced by the defect.

Continuum model of the fullerenes.



792

J. González et al. / Electronic spectrum of fullerenes

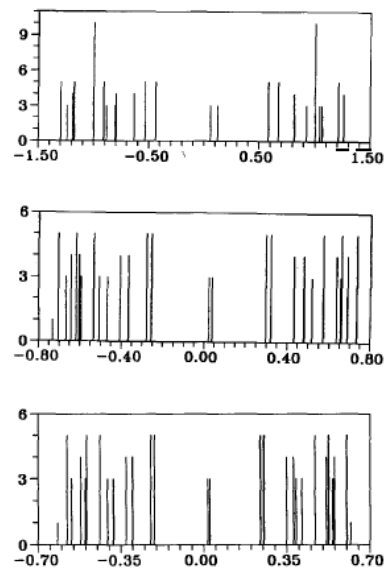


Fig. 8. Spectra of honeycomb lattices on the icosahedron. Energy eigenvalues are plotted in the horizontal axis and the multiplet degeneracy is given along the vertical direction as in fig. 7. The diagrams correspond, respectively, to the lattices C₂₄₀, C₉₆₀ and C₁₅₀₀.

- Dirac equation on a spherical surface.
- Constant magnetic field (Dirac monopole).

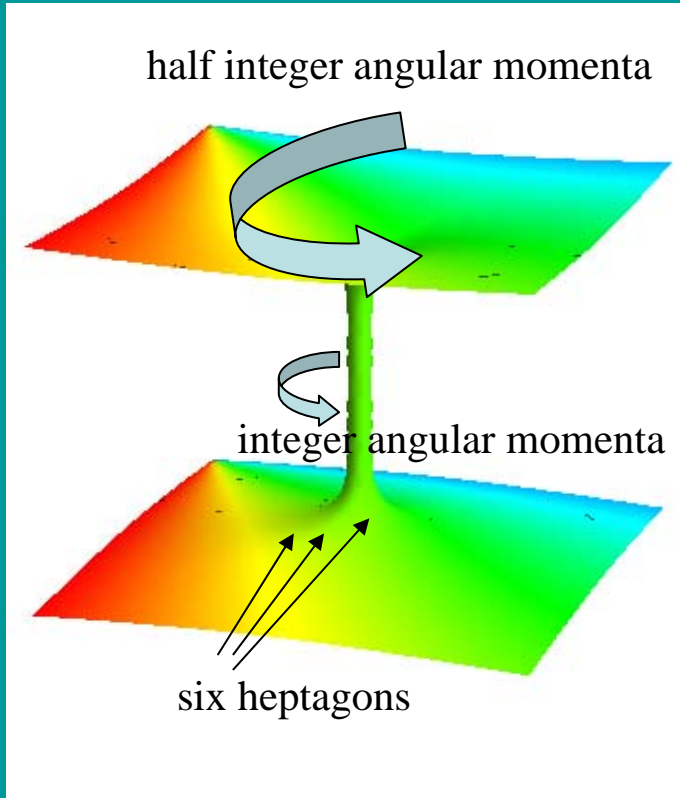
$$\frac{\hbar v_F}{R} \left[i\partial_\theta - \frac{1}{\sin(\theta)} \partial_\phi + \frac{i(1+l)\cos(\theta)}{2\sin(\theta)} \right] \Psi_a = \varepsilon \Psi_b$$

$$\frac{\hbar v_F}{R} \left[i\partial_\theta + \frac{1}{\sin(\theta)} \partial_\phi + \frac{i(1-l)\cos(\theta)}{2\sin(\theta)} \right] \Psi_b = \varepsilon \Psi_a$$

$$\varepsilon_J = \frac{\hbar v_F}{R} \sqrt{[J(J+1)] - l(l+1)} \quad J \geq l$$

Topological defects

J. González, F. G., J. Herrero, arXiv:0901.1557



Fujitsu Achieves Breakthrough with World's First New Carbon Nanotube Composite

- Features self-organizing carbon nanotubes and graphene -

Atsugi, Japan, March 3, 2008 — Fujitsu Laboratories Ltd. today announced the successful formation of a new nano-scale carbon composite featuring a self-organizing structure⁽¹⁾, by combining carbon nanotubes and graphene⁽²⁾ which are both nano-scale carbon structures. The newly-discovered composite structure is synthesized at a temperature of 510 °C, cooler than for conventional graphene formed at temperatures too high for electronic device applications, thereby paving the way for the feasible use of graphene as a material suitable for future practical use in electronic devices which are vulnerable to heat. Carbon nanotubes have properties including high thermal conductivity and high current-density tolerance⁽³⁾, while graphene is known for its high electron mobility. Carbon nanostructures combining these two materials hold the promise of creating new potential for material research and applications.

Details of this technology will be presented at the 34th Fullerene Nanotubes General Symposium to be held from March 3 to March 5 in Nagoya, Japan.

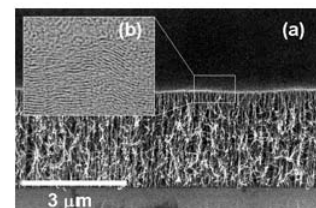
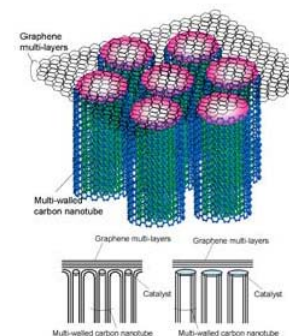


Figure 1. (a) Electron microscopic image (cross-sectional) of the new nano-scale carbon composite
(b) Electron microscopic image of the graphene multi-layers

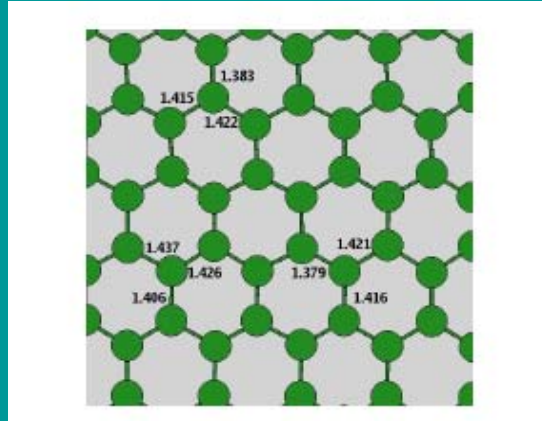


[Larger View](#)

Figure 2. Schematic view of the new nano-scale carbon composite (Lower image: Diagram of anticipated structure)

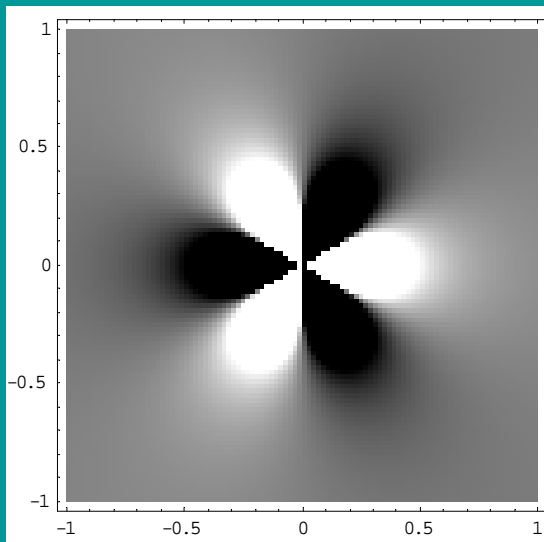
Effective gauge fields

In plane elastic deformations



A. Fasolino, J. H. Los, and M. I. Katsnelson, Nature Mat. **6**, 858 (2007)

Elastic strains imply deformations of bonds,
and modulations of hoppings.



Effective
magnetic
field
induced
around a
dislocation.

H. Suzuura and T. Ando, Phys. Rev. B **65**, 235412 (2002)
J. L. Mañes, Phys. Rev. B **76**, 045430 (2007)

$$H \equiv \begin{pmatrix} 0 & v_F(k_x + ik_y) + \beta t(u_{xx} - u_{yy} - 2iu_{xy}) \\ v_F(k_x - ik_y) + \beta t(u_{xx} - u_{yy} + 2iu_{xy}) & 0 \end{pmatrix}$$

$$\beta = \frac{\partial \log(t)}{\partial \log(a)} \approx 2$$

$$\frac{\partial^2 u_{ij}}{\partial x_k \partial x_l} + \frac{\partial^2 u_{kl}}{\partial x_i \partial x_j} - \frac{\partial^2 u_{il}}{\partial x_j \partial x_k} - \frac{\partial^2 u_{jk}}{\partial x_i \partial x_l} = 0$$

$$R_{ijkl} = \frac{1}{2} \left(\frac{\partial^2 g_{ij}}{\partial x_k \partial x_l} + \frac{\partial^2 g_{kl}}{\partial x_i \partial x_j} - \frac{\partial^2 g_{il}}{\partial x_j \partial x_k} - \frac{\partial^2 g_{jk}}{\partial x_i \partial x_l} \right) + O(g^2)$$

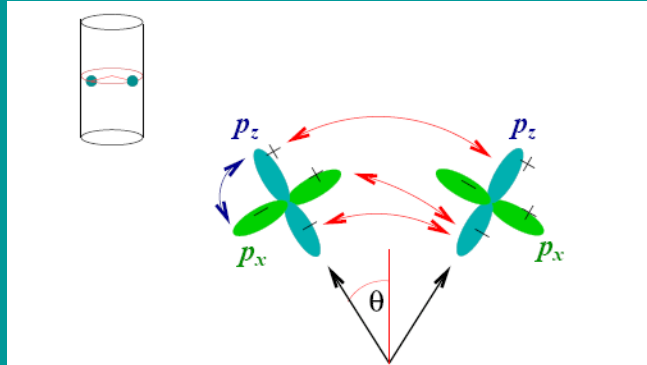
Saint Venant's compatibility conditions
imply zero intrinsic curvature

The gauge field associated
to elastic strains is material
dependent, and it does not
imply intrinsic curvature.

Effective gauge fields

Misalignment of π orbitals

A. H. Castro Neto and E.-A. Kim, Europhys. Lett. **84**, 57007 (2008),
 see also E. Mariani and F. von Oppen, Phys. Rev. Lett. **100**, 249991 (2008)



A finite curvature induces the mixing of π and σ orbitals, and modifies the effective hoppings.

$$\delta t \approx \left(-\frac{1}{3} t_{pp\pi} + \frac{1}{2} t_{pp\sigma} \right) [(\vec{a}\nabla)\nabla h]^2$$

$$A_x \propto \left(\frac{\partial^2 h}{\partial x^2} \right)^2 - \left(\frac{\partial^2 h}{\partial y^2} \right)^2$$

$$A_y \propto -2 \frac{\partial^2 h}{\partial x \partial y} \left(\frac{\partial^2 h}{\partial x^2} + \frac{\partial^2 h}{\partial y^2} \right)$$

The gauge field associated to the misalignment of π orbitals is material dependent, and it does not imply intrinsic curvature.

Non abelian gauge potential II.

$$\begin{array}{cccc}
 |KA\rangle & |KB\rangle & |K'A\rangle & |K'B\rangle \\
 \begin{array}{c} |KA\rangle \\ |KB\rangle \\ |K'A\rangle \\ |K'B\rangle \end{array} \left(\begin{array}{cccc} 0 & v_F(k_x - ik_y) & v_F[-iA_x(\vec{r}) - A_y(\vec{r})] & 0 \\ v_F(k_x + ik_y) & 0 & 0 & v_F[iA_x(\vec{r}) - A_y(\vec{r})] \\ v_F[iA_x(\vec{r}) - A_y(\vec{r})] & 0 & 0 & v_F(k_x + ik_y) \\ 0 & v_F[-iA_x(\vec{r}) - A_y(\vec{r})] & v_F(k_x - ik_y) & 0 \end{array} \right)
 \end{array}$$

Dirac hamiltonian for the two valleys, with Umklapp scattering.

$$\begin{array}{cccc}
 |KA\rangle + i|K'B\rangle & |KB\rangle - i|K'A\rangle & |KA\rangle - i|K'B\rangle & |KB\rangle + i|K'A\rangle \\
 \begin{array}{c} |KA\rangle + i|K'B\rangle \\ |KB\rangle - i|K'A\rangle \\ |KA\rangle - i|K'B\rangle \\ |KB\rangle + i|K'A\rangle \end{array} \left(\begin{array}{cccc} 0 & v_F(k_x + A_x - ik_y - iA_y) & 0 & 0 \\ v_F(k_x + A_x + ik_y + iA_y) & 0 & 0 & 0 \\ 0 & 0 & 0 & v_F(k_x - A_x + ik_y - iA_y) \\ 0 & 0 & v_F(k_x - A_x - ik_y + iA_y) & 0 \end{array} \right)
 \end{array}$$

Intervalley scattering acts as a gauge potential which rotates the valley index.
It plays a similar role to the potential induced by pentagons and heptagons.

Gauge potentials

Physical origin

Elastic strains

Mixing of σ and π bands (extrinsic curvature)

Topological defects (intrinsic curvature)

Effects

Elastic strains

Intravalley scattering

Intervalley scattering (non commuting gauge fields)

Strains also induce scalar potentials, S. Ono and K. Sugihara, Journ. Phys. Soc. Jap. **61**, 861 (1966), H. Suzuura and T. Ando, Phys. Rev. B **65**, 235412 (2002), see also J. Jiang , R. Saito, A. Grüneis, G. Dresselhaus, M.S. Dresselhaus, Chem. Phys. Lett. 392, 383 (2004), T. O. Wehling, A. V. Balatsky, A. M. Tsvelik, M. I. Katsnelson, and A. I. Lichtenstein, Europhys. Lett. **84**, 17003 (2008))

Scalar potentials which vary on scales longer than $\lambda_{\text{FT}} \sim k_F^{-1}$ will be screened

Ripples in graphene

J. C. Meyer, A. K. Geim, M. I. Katsnelson, K. S. Novoselov, T. J. Booth and S. Roth,
Nature **446**, 60 (2007).

J. C. Meyer, A. K. Geim, M. I. Katsnelson, K. S. Novoselov, D. Obergfell, S. Roth, C. Girit
 and A. Zettl, *Sol. St. Commun.* **143**, 101 (2007).

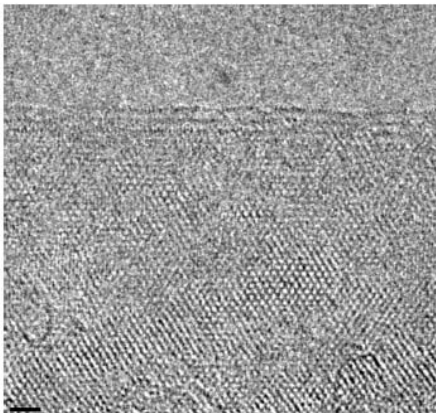


Figure 4 | Atomic resolution imaging of graphene membranes. TEM image of a few-layer graphene membrane near its edge, where the number of dark lines indicates the thickness of two to four layers. Because for few-layer graphene the electron contrast depends strongly on incidence angle, relatively small (a few degrees) variations in the surface normal become visible. The atomic-resolution imaging was achieved by using FEI Titan at an acceleration voltage of 300 kV. Scale bar, 1 nm.

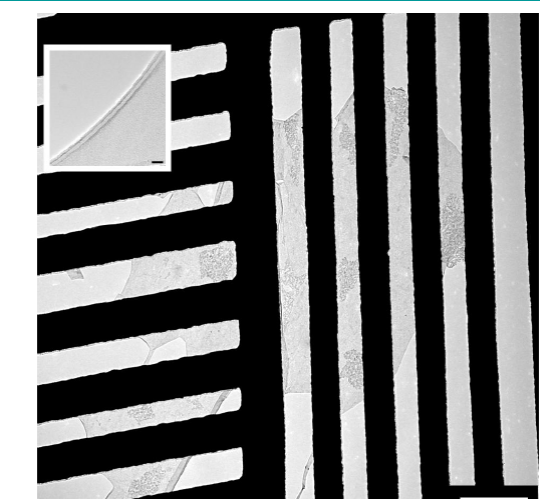


Figure 1: TEM image of suspended graphene (darker gray areas) supported by a microfabricated metal grid (black lines). The inset shows a scroll at the edge. Scale bar 1 μ m, and 20 nm for the inset.

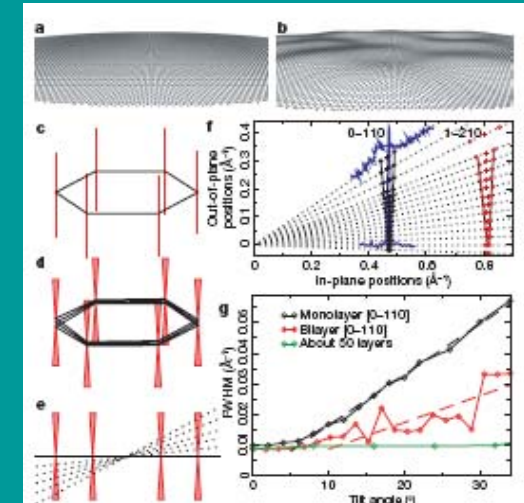
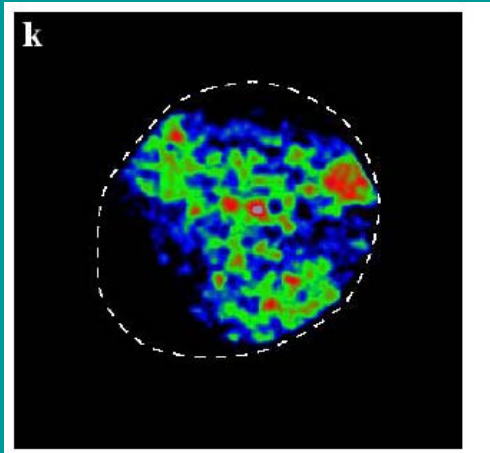


Figure 3 | Microscopically corrugated graphene. **a**, Flat graphene crystal in real space (perspective view). **b**, The same for corrugated graphene. The roughness shown imitates quantitatively the roughness found experimentally. **c**, The reciprocal space for a flat sheet is a set of rods (red) directed perpendicular to the reciprocal lattice of graphene (black hexagon). **d**, **e**, For the corrugated sheet, a superposition of the diffracting beams from microscopic flat areas effectively turns the rods into cone-shaped volumes so that diffraction spots become blurred at large angles (indicated by the dotted lines in **e**) and the effect is more pronounced further away from the tilt axis (compare with Fig. 2). Diffraction patterns obtained at different tilt angles allow us to measure graphene roughness. **f**, Evolution of diffraction peaks with tilt angle in monolayer graphene. The experimental data are presented in such a way that they closely resemble the schematic view in **e**. For each tilt angle, the black dotted line represents a cross-section for diffraction peaks (0-110) and (1-210). The peak centres and full widths at half maxima (PWHM) in reciprocal space are marked by crosses and open circles, respectively. In two cases (0° and 34°), the recorded intensities are shown in full by blue curves. All the intensity curves could be well fitted by the gaussian shape. The solid black lines show that the width of the diffraction spots reproduces the conical broadening suggested by our model (**d** and **e**). **g**, PWHM for the (0-110) diffraction peak in monolayer and bilayer membranes and thin graphite (as a reference), as a function of tilt angle. The dashed lines are the linear fits yielding the average roughness. The flat region between 0° to 5° , and also for the reference sample, is due to the intrinsic peak width for the microscope at our settings.

Ripples in graphene

Single layer graphene on SiO₂

M. Ishigami, J. H. Chen, W. G. Cullen, M. S. Fuhrer and E. D. Williams, Nano Letters **7**, 6 (2007)

E. Stolyarova, K. T. Rim, S. Ryu, J. Maultzsch, P. Kim, L. E. Brus, T. F. Heinz, M. S. Hybertsen and G. W. Flynn, Proc. Nat. Acad. Sci. **104**, 9209 (2007)

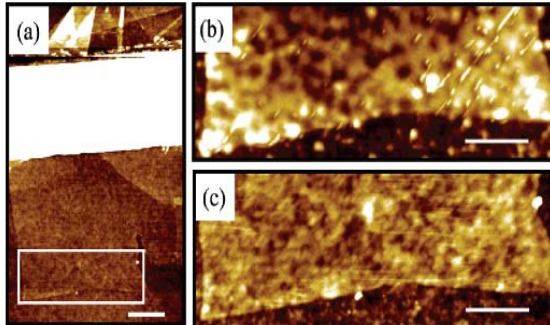


Figure 2. (a) AFM topography of graphene deposited on SiO₂. Thin graphite flakes are generated using the mechanical exfoliation technique¹ on thermally grown SiO₂ with the thickness of 300 nm. Monolayer graphite flakes (graphene) are located using optical and atomic force microscopy.² The e-beam lithography defined electrode,³³ approximately 80 nm in height and 1.5 μ m in width, is the white area nearly horizontal to the image. The black square indicates the region shown in parts b and c of Figure 1. The scale bar is 500 nm. (b) Graphene sheet prior to the cleaning procedure described in text. The scale bar is 300 nm. (c) Graphene sheet after the cleaning procedure. The standard deviation of the height variation in a square of side 600 nm is approximately 3 Å after the treatment compared to 8 Å before the treatment. The scale bar is 300 nm. Images a–c were acquired using intermittent-contact mode AFM in air.

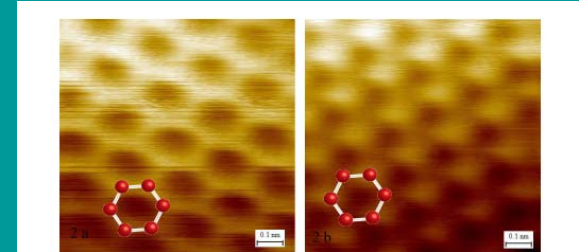
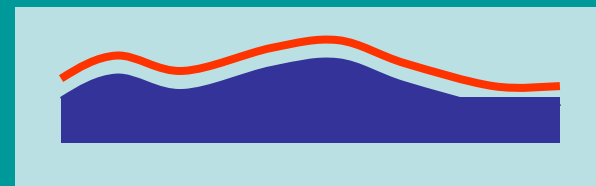
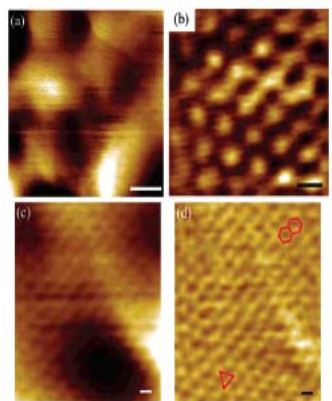


Figure 2. STM topographic images of different regions of the graphene flake of Fig. 1. The images were obtained with $V_{bias} = +1V$ (sample potential), $I=1\text{ nA}$, and a scan area of 1 nm^2 . A model of the underlying atomic structure is shown as a guide to the eye. (a) Image from a single-layer of graphene (region I of Fig. 1). A honeycomb structure is observed. (b) Image of the multi-layer portion of the sample (region II of Fig 1). The characteristic “three-for-six” STM image of the surface of bulk graphite is observed.



The graphene layer follows the corrugation of the substrate

Figure 3. (a) A typical large-area STM image of the graphene sheet shown in Figure 2a. Peak-to-peak height variation of the image is approximately 2.3 Å. $V_{bias}=+1V$ and $I=0.3\text{ nA}$. The scale bar is 2 nm. (b) A schematically rendered image of a graphene sheet, $P_{corr}=1.3\text{ V}$, $I=0.3\text{ nA}$. The red line is the profile of the surface of the substrate. The scale bar is 2.5 Å. $V_{bias}=+1.1\text{ V}$ and $I=0.6\text{ nA}$. (c) A high-power AFM image of the large area scan shown in (a). Both trigonal and hexagonal patterns are observed. The orientation of the red triangle and hexagons are same. The scale bar is 2.5 Å.

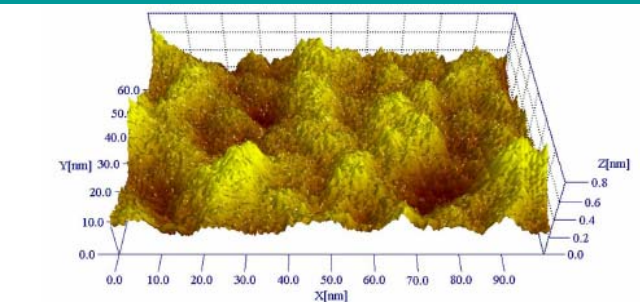


Figure 3. Stereographic plot of a large-scale ($100\times62\text{ nm}$) STM image of a single-layer graphene film on the silicon dioxide surface. The STM scanning conditions were: $V_{bias}=1\text{ V}$ (sample potential) and $I=0.6\text{ nA}$. The 0.8-nm scale of the vertical (Z) coordinate is greatly enlarged to accentuate the surface features.

Effective gauge fields induced by random corrugations

Effective magnetic length:

$$l_B \propto \begin{cases} l \left(\frac{l}{h} \right) \\ l \sqrt{\frac{t}{E}} \frac{l^3}{ah^2} \\ l \sqrt{\left(\frac{\partial \log(t)}{\partial \log(a)} \right)^{-1}} \frac{al}{h^2} \end{cases}$$

Intrinsic curvature

Mixing between π and σ orbitals

Elastic strains

Some estimates: $h=1\text{nm}$, $l=10\text{nm}$, $a=0.1\text{nm}$

$$l_B \approx \begin{cases} 100\text{nm} & B \approx 0.06T \\ 1000\text{nm} & B \approx 0.0006T \\ 10\text{nm} & B \approx 6T \end{cases}$$

Intrinsic curvature

Mixing between π and σ orbitals

Elastic strains

Weak (anti)localization in graphene

A. Morpurgo and F. G., Phys. Rev. Lett. **97**, 196804 (2006)

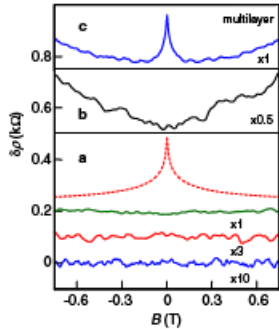


FIG. 2 (color online). (a) Many graphene devices exhibited no sign of weak localization or antilocalization. Solid curves correspond to gate voltages shown by arrows in Fig. 1 (≈ 10 , 20, and 50 V from top to bottom curve, respectively). The curves are shifted for clarity ($\rho \approx 1.5$, 0.8, and 0.4 $\text{k}\Omega$ from top to bottom). The lowest curve corresponds to $k_F \approx 50$. Notice magnification factors for the $\delta\rho$ scale against each of the curves. These factors were chosen so that the expected WL peak for all the curves would be of approximately the same size as the peak shown by the dashed curve calculated using the standard WL theory [11,12]. (b) Magnetoresistance behavior at zero V_g , where ρ reaches its maximum $\approx 6 \text{k}\Omega$. For such high resistivity (i.e., $\approx h/e^2$ per each type of carriers), a metal-insulator transition is generally expected but it does not occur in the case of graphene [2]. Both absolute value of ρ and its magnetoresistance $\delta\rho(B)$ are practically temperature independent below 100 K. (c) Multilayer films [10] exhibited the standard weak-localization behavior. Shown is a device with $\rho \approx 1.2 \text{k}\Omega$ and mobility $\approx 10\,000 \text{ cm}^2/\text{Vs}$ (no gate voltage applied). A clear WL peak is seen at zero B . In higher fields, multilayer devices exhibit a large linear ($\propto B$) magnetoresistance. All curves shown in Fig. 2 were measured at 4 K.

Gauge fields
break the effective
time reversal
invariance at each
valley:
antilocalization
effects are
suppressed

S. V. Mozorov, K. S. Novoselov, M. I. Katsnelson, F. Schedin, D. Jiang, and A. K. Geim, Phys. Rev. Lett. **97**, 016801 (2006)

See also E. McCann, K. Kechedzhi, V. I. Fal'ko, H. Suzuura, T. Ando and B. L. Altshuler, Phys. Rev. Lett. **97**, 146805 (2006).
X. Wu, X. Li, Z. Song, C. Berger and W. A. de Heer, Phys. Rev. Lett. **93**, 136801 (2007).

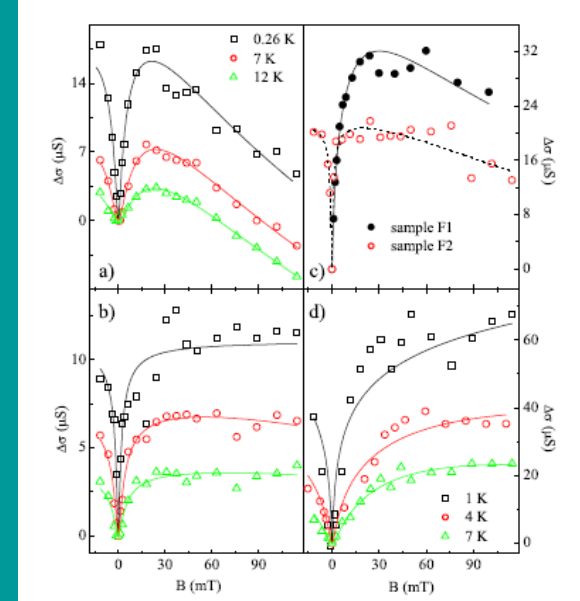


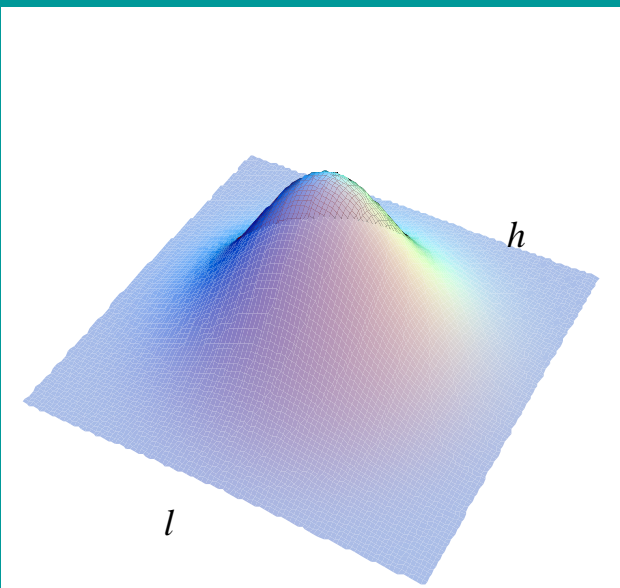
FIG. 2: Magnetoconductivity observed in graphene flakes. (a) Dirac region of sample D, $|V_g| \lesssim 1 \text{ V}$, $n \lesssim 7 \times 10^{10} \text{ cm}^{-2}$; (b) sample D, $V_g \approx 14 \text{ V}$, $n \approx 10^{12} \text{ cm}^{-2}$ (the legends of (a) and (b) are the same); (c) samples F1 and F2 at $T = 1 \text{ K}$, $V_g \approx 10 \text{ V}$, $n \approx 7 \times 10^{11} \text{ cm}^{-2}$; (d) sample B, $V_g \approx 11 \text{ V}$, $n \approx 8 \times 10^{11} \text{ cm}^{-2}$. Lines are best fits to Eq. 1.

F. V. Tikhonenko, D. W. Horsell, D. V. Gorbachev, and A. K. Savchenko, Phys. Rev. Lett. **100**, 056802 (2008)

Scattering by ripples

16

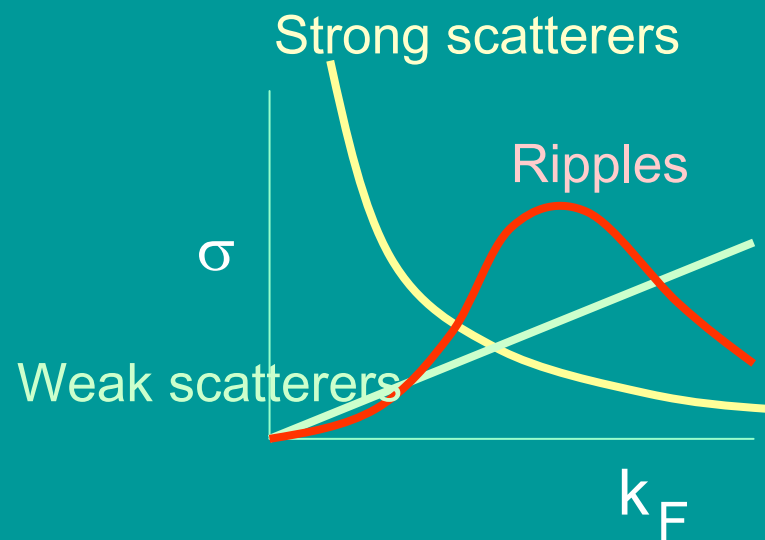
F. G. J. Low Temp. Phys. **153**, 359 (2008)



Born approximation

$$\sigma(\theta) \propto \{1 + \cos[3(\theta_{out} + \theta_{in})]\} \times \begin{cases} \left(\frac{\partial \log(t)}{\partial \log(a)}\right)^2 \frac{k_F h^4 (k_F l)^4}{a^2} & k_F l \ll 1 \\ \left(\frac{\partial \log(t)}{\partial \log(a)}\right)^2 \frac{k_F h^4}{a^2} & k_F l \approx 1 \\ \left(\frac{\partial \log(t)}{\partial \log(a)}\right)^2 \frac{k_F h^4}{a^2 (k_F l)^4} & k_F l \gg 1 \end{cases}$$

- The cross section does not have a monotonous dependence on the carrier density.
- The angular dependence reflects the trigonal symmetry of the lattice.

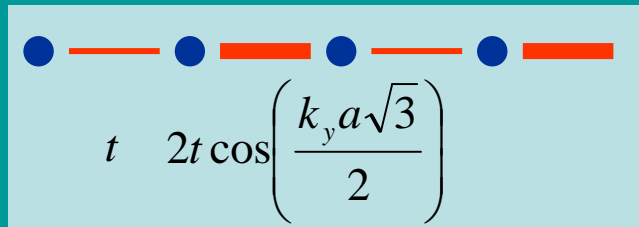
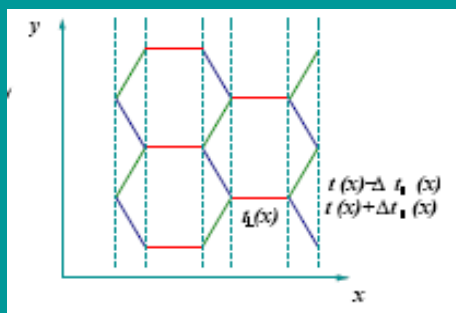
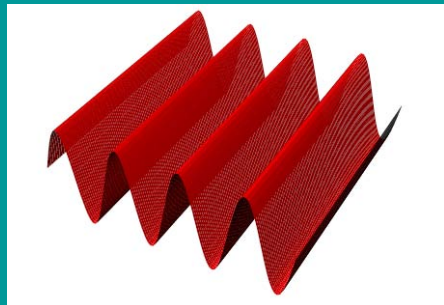


Model of the electronic structure of rippled graphene

17

F. G., M. I. Katsnelson, M. A. H. Vozmediano, Phys. Rev. B 77, 075422 (2008)

see also T. O. Wehling, A. V. Balatsky, A. M. Tsvelik, M. I. Katsnelson, and A. I. Lichtenstein, Europhys. Lett. 84, 17003 (2008)



Effective 1D model with two hoppings

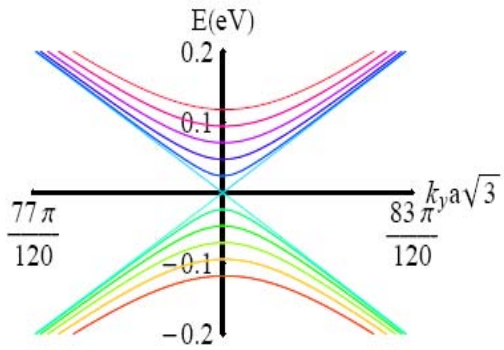
$$\begin{aligned} t &\leftrightarrow t_{\parallel}(x) \\ 2t \cos\left(\frac{k_y a \sqrt{3}}{2}\right) &\leftrightarrow \sqrt{\bar{t}_{\perp}^2(x) \cos^2\left(\frac{k_y a \sqrt{3}}{2}\right) + \Delta t_{\perp}^2(x) \sin^2\left(\frac{k_y a \sqrt{3}}{2}\right)} \end{aligned}$$

Modulation of the hoppings

$$\begin{aligned} t &\leftrightarrow t \\ 2t \cos\left(\frac{k_y a \sqrt{3}}{2}\right) &\leftrightarrow 2t \cos\left(\frac{(k_y + A_y(x))a \sqrt{3}}{2}\right) \end{aligned}$$

Effect of a magnetic field

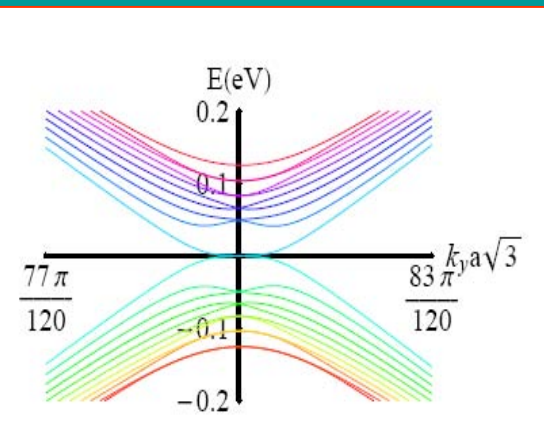
Results



$\delta t/t=0$

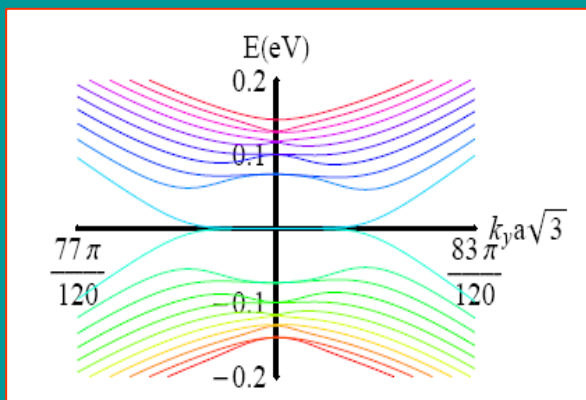
There are well defined midgap levels

$$t_{\parallel}(x) = \delta t \sin\left(\frac{2\pi x}{l}\right)$$



$\delta t/t=0.02$

The Dirac bands are recovered at high energies.



$\delta t/t=0.04$

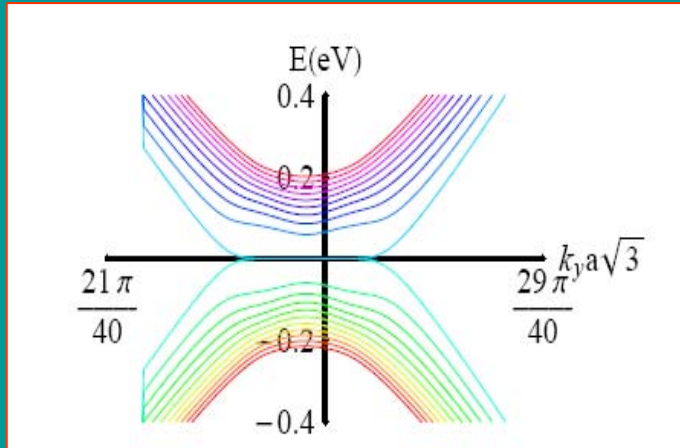
$$l_B \approx \sqrt{\frac{t}{\delta t}} la$$

$$\Delta \approx t \sqrt{\frac{\delta t}{t} \frac{a}{l}}$$

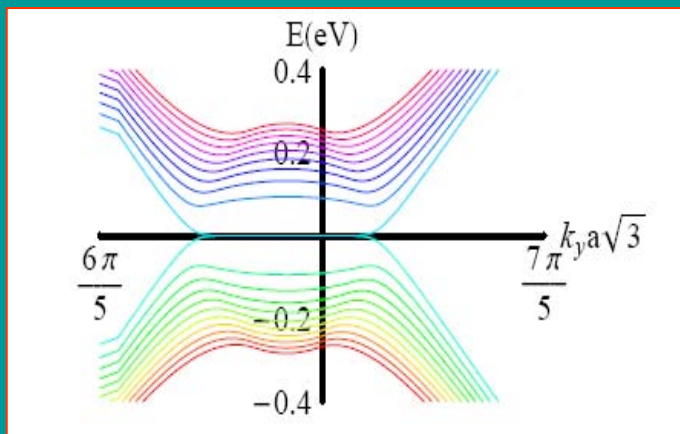
$l=1200$ $a=168$ nm

Results. (Real) magnetic fields

$B=10\text{T}$, $\delta t/t=0.02$



K point



K' point

See also: E. Perfetto, J. González, F. G., S. Bellucci and P. Onorato, Phys. Rev. B **76**, 125430 (2006)

A real magnetic field breaks the symmetry between the two valleys: valleytronics.

A. Rycerz and J. Tworzydo and C. W. J. Beenakker, Nature Physics **3**, 172 (2007)

Electrons move around different cyclotron orbits, and are deflected differently by barriers.

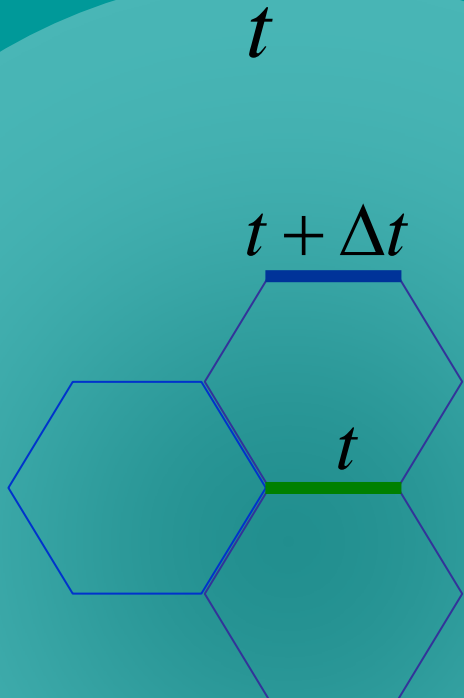
V. V. Cheianov and V. I. Fal'ko, Phys. Rev. B **74**, 041403 (2006)

Effective flux through a ripple

20

F. G., M. I. Katsnelson and M. A. H. Vozmediano, Phys. Rev. B **77**, 075422 (2008)

$$l$$



$$\beta = \frac{\partial \log(t)}{\partial \log(a)} \approx 2 - 3$$

$$\frac{\Delta t}{t} \approx \beta \bar{u} \approx \begin{cases} \beta \left(\frac{h}{l} \right)^2 & \text{Out of plane corrugations} \\ \beta \frac{\Delta a}{a} & \text{In plane displacements} \end{cases}$$

$$\Delta t \approx v_F |\vec{A}|$$

$$l_B^2 \approx \frac{la}{\beta \bar{u}}$$

$$\Phi \approx \beta \bar{u} \frac{l}{a} \approx \begin{cases} \beta \frac{h^2}{la} \\ \beta \frac{\Delta al}{a^2} \end{cases}$$

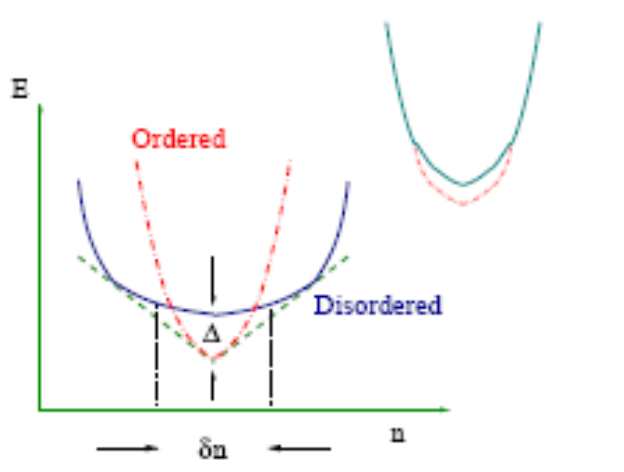
Φ is the number of Landau levels that fit into one ripple

Electron-electron interactions.

The electronic compressibility in clean graphene is zero. The electronic compressibility in graphene with ripples can be very large:

$$\kappa \approx \frac{e^\Phi}{\Delta l_B^2} \approx \frac{e^{\delta t/ta}}{ta} \sqrt{\frac{\delta t}{ta}}$$

The $n=0$ Landau level leads to many instabilities, see
 M. O. Goerbig, R. Moessner and B. Doucot, Phys. Rev. B **74**, 161407 (2006)
 K. Nomura and A. H. MacDonald, Phys. Rev. Lett. **96**, 256602 (2006)
 H. A. Fertig and L. Brey, Phys. Rev. Lett. **97**, 116805 (2006)
 J. Alicea and M. P. A. Fisher, Phys. Rev. B **74**, 075422 (2006)
 V. P. Gusynin and V. A. Miransky and S. G. Sharapov and I. A. Shovkovy, Phys. Rev. B **74**, 195429 (2006)
 V. A. Apalkov and T. Chakraborty, Phys. Rev. Lett. **97**, 126801 (2006)
 J.-N. Fuchs and P. Lederer, Phys. Rev. Lett. **98**, 016803 (2007)
 D. A. Abanin, K. S. Novoselov, U. Zeitler, P. A. Lee, A. K. Geim and L. S. Levitov, Phys. Rev. Lett. **98**, 196806 (2007)
 V. Lukose and R. Shankar, arXiv:0706.4280



Electronic interactions will induce magnetic or charge ordering.
 The high electronic compressibility favors a first order transition and electronic phase separation.

F. G., G. Gómez-Santos and D. P. Arovas, Phys. Rev. B **62**, 391 (2002)

An obvious possibility is a ferromagnetic state.

Dirac electrons in a random gauge field

22

- A. W. Ludwig, M. P. A. Fisher, R. Shankar, and G. Grinstein, Phys. Rev. B **50**, 7526 (1994)
 B. Horovitz and P. Le Doussal, Phys. Rev. B **65**, 125323 (2002)
 F. G., P. Le Doussal, B. Horovitz, Phys. Rev. B **77**, 205421 (2008)

Random gauge disorder.

$$\langle \vec{A}(\vec{r}), \vec{A}(\vec{r}') \rangle = \sigma \delta^{(2)}(\vec{r} - \vec{r}')$$

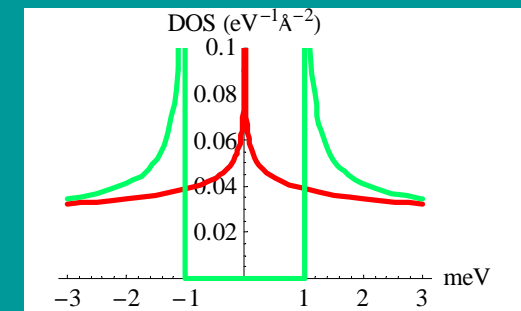
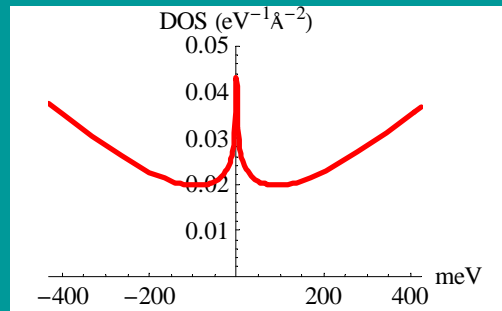
$$|\vec{r} - \vec{r}'| \gg l$$

$$\rho(\varepsilon) \propto \varepsilon^{2/z-1}$$

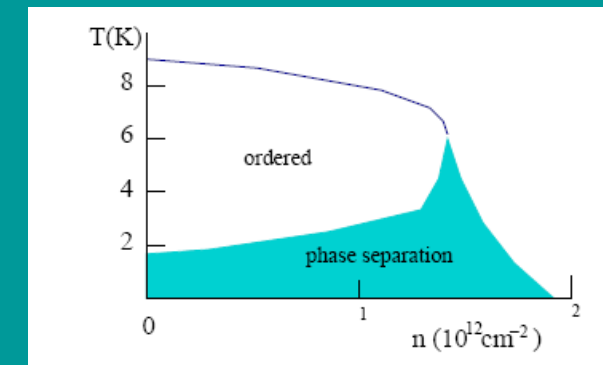
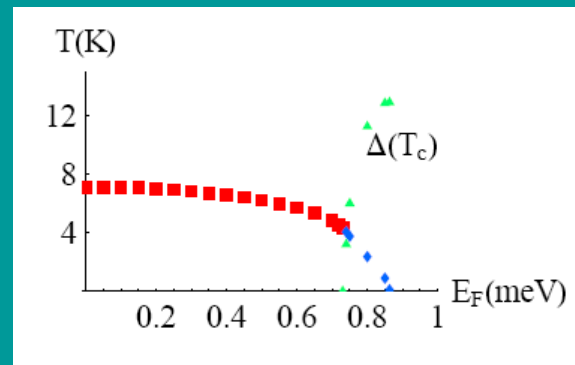
$$z = \begin{cases} 2 - K + \sigma K^2 & \sigma < \frac{1}{2K^2} \\ K(\sqrt{8\sigma} - 1) & \sigma > \frac{1}{2K^2} \end{cases}$$

For ripples, the strength of the divergence is controlled by a dimensionless parameter:

$$\sigma \propto \beta^2 \frac{h^4}{l^2 a^2}$$



The density of states diverges for sufficiently large disorder.
 Short range interactions become relevant.
 A gap, Δ , can be induced



Ordered phase at low temperatures.
 The transition is first order, leading to electronic phase separation

Electrostatic interactions and disorder.

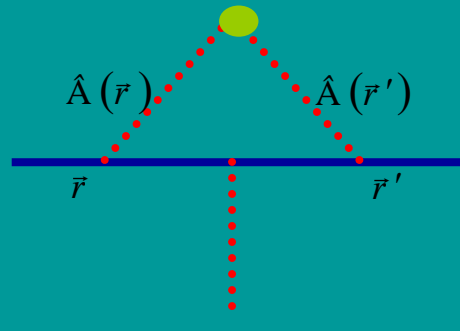
T. Stauber, F. G. and M. A. H. Vozmediano, Phys. Rev. B **71**, 041406 (2005)

J. Ye, Phys. Rev. B **60**, 8290 (1999).

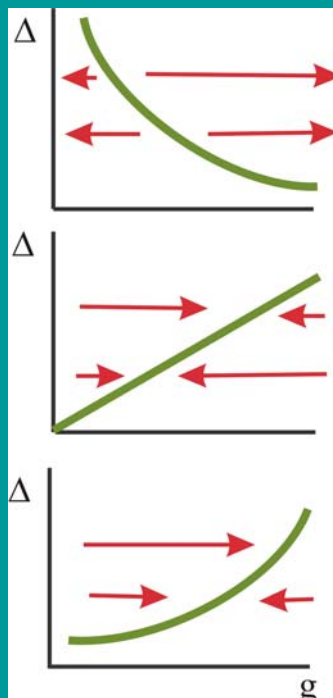
M. S. Foster and A. W. W. Ludwig, Phys. Rev. B **73**, 155104 (2006), *ibid* **74**, 241102(R) (2006)

M. S. Foster and I. L. Aleiner, Phys. Rev. B **77**, 195413 (2008)

I. F. Herbut, V. Juricic, and O. Vafek, Phys. Rev. Lett. **100**, 046403 (2008)



- There are selfenergy and vortex corrections.
- The selfenergy induces wavefunction renormalization.
- The vortex corrections depend on the type of disorder.
- The wavefunction renormalization changes the flow of the coupling constant.



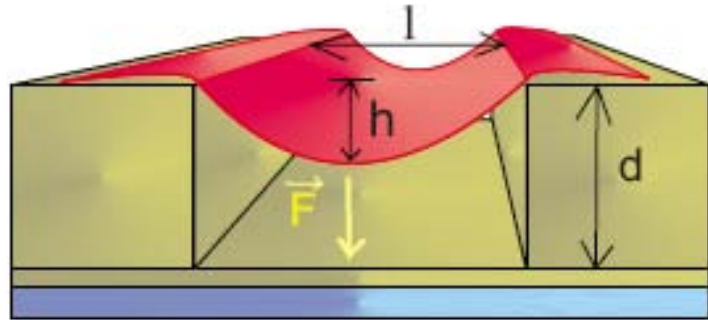
Smooth random potential

Coarse grained lattice defects

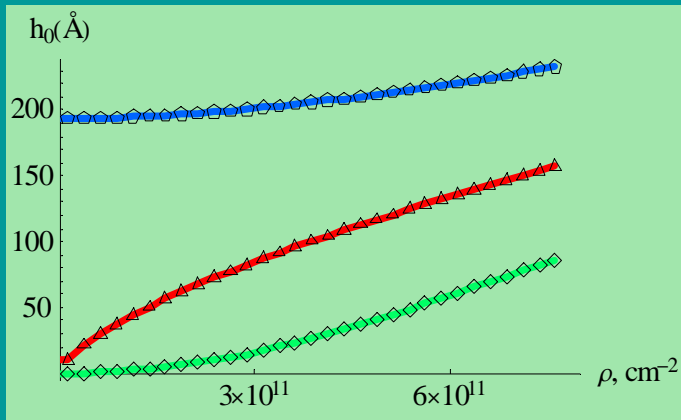
Smooth staggered potential

Ballistic transport in suspended graphene

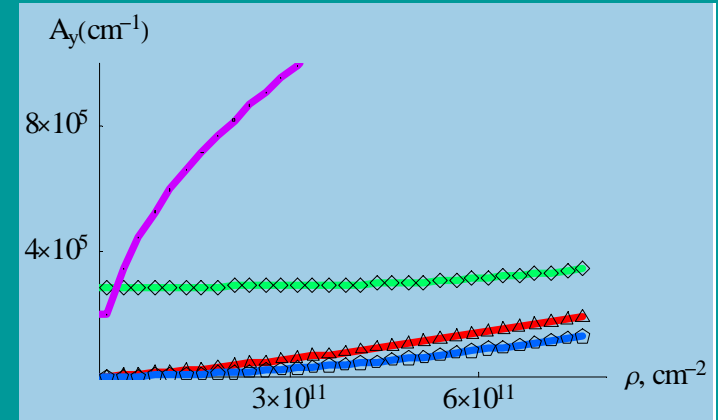
M. M. Fogler, F. G., M. I. Katsnelson, ArXiv: 0807.3165



- The graphene layer is deformed by the applied electric field, slack, ...
- Stresses lead to effective gauge potentials



Maximum height as function of carrier density for different values of the slack

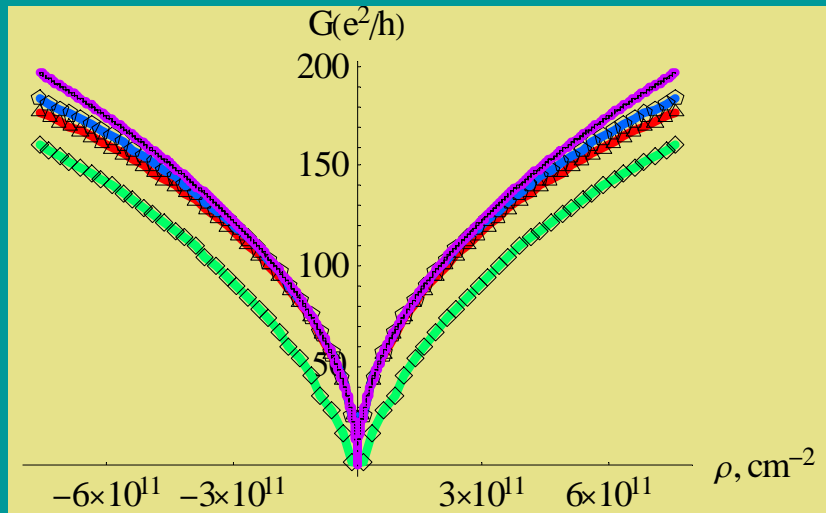


Vector potential inside the suspended region as function of carrier density for different values of the slack

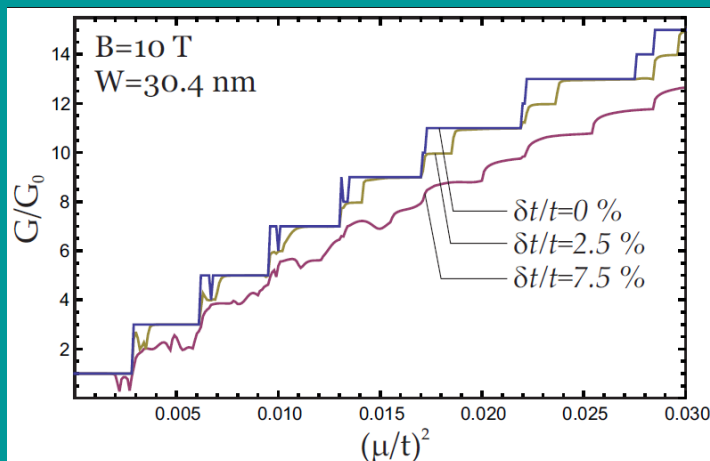
Ballistic transport in suspended graphene

25

M. M. Fogler, F. G., M. I. Katsnelson, Phys. Rev. Lett. **101**, 226804 (2008)



Transmission through a deformed graphene sheet as function of density for different values of the slack



Integer Quantum Hall steps in a graphene ribbon where part of it is under a constant stress

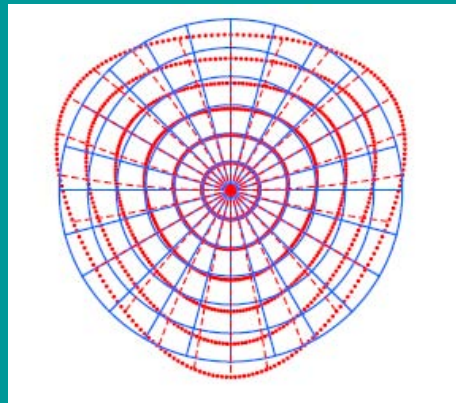
G. León, E. Prada, P. San José, F. G., unpublished

Effective magnetic fields in strained graphene

A. K. Geim, M. I. Katsnelson, F. G., unpublished

$$\begin{aligned} u_r(r, \theta) &= Ar^2 \sin(3\theta) \\ u_\theta(r, \theta) &= Ar^2 \cos(3\theta) \\ \sigma_{rr}(r, \theta) &= 4\mu Ar \sin(3\theta) \\ \sigma_{\theta\theta}(r, \theta) &= -4\mu Ar \sin(3\theta) \\ \sigma_{r\theta}(r, \theta) &= 4\mu Ar \cos(3\theta) \end{aligned}$$

$$\begin{aligned} u_x(x, y) &= 2Axy \\ u_y(x, y) &= A(x^2 - y^2) \\ \sigma_{xx}(x, y) &= 4\mu Ay \\ \sigma_{yy}(x, y) &= -4\mu Ay \\ \sigma_{xy}(x, y) &= 4\mu Ax \end{aligned}$$



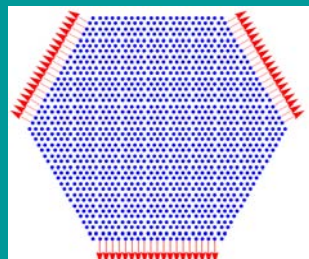
$$l_B \approx \sqrt{\frac{aR}{8\bar{u}\beta}}$$

$$R \approx 1\mu m, \quad a \approx 0.1 nm, \quad \beta \approx 3, \quad \bar{u} \approx 0.1$$

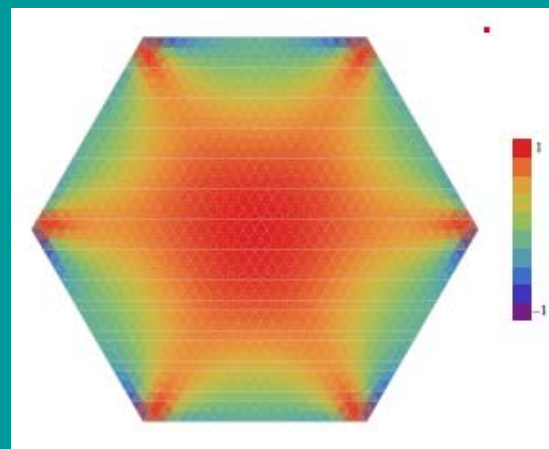
$$l_B \approx 7 nm, \quad B \approx 10 T$$

Shear deformation:
Constant effective
magnetic field

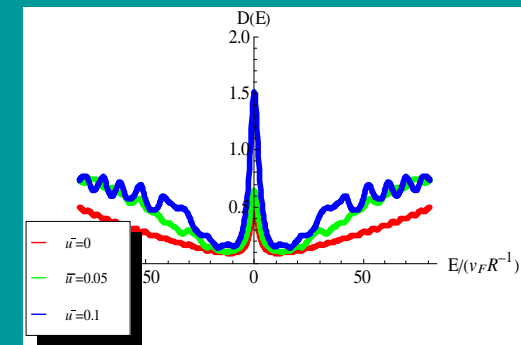
Applied forces



Dependence on
boundary
conditions:



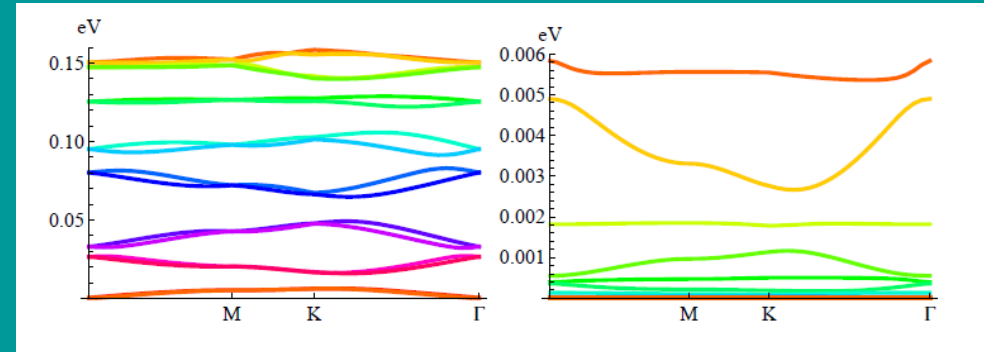
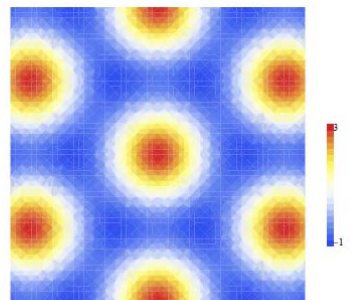
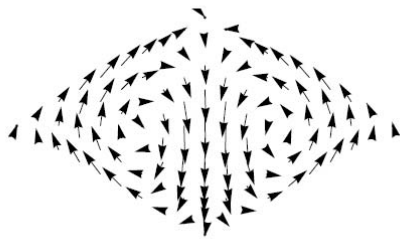
Effective magnetic field



Total density of states

Strain superlattices

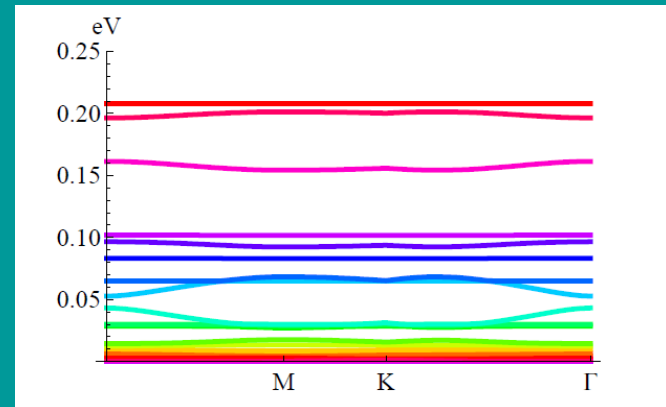
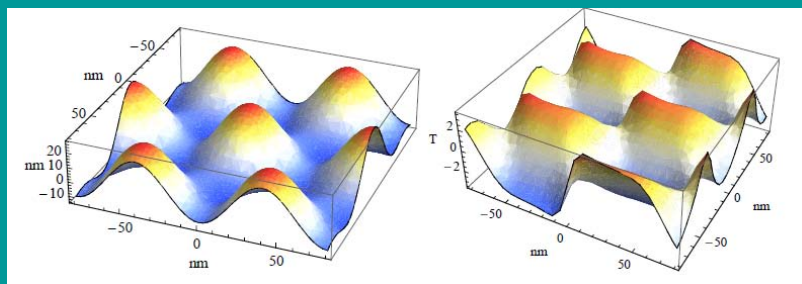
27



In plane displacements

$$\bar{u} = 0.005$$

$$\bar{u} = 0.01$$



Height modulations

Wrinkles and mechanical instabilities in strained graphene²⁸

F. G., B. Horovitz, P. Le Doussal, arXiv:0811.4670, Solid St. Commun., in press

Wrinkling instability: E.Cerda and L. Mahadevan, Phys. Rev. Lett. **90**, 074302 (2003)
T. A. Witten, Rev. Mod. Phys. **79**, 643 (2007)

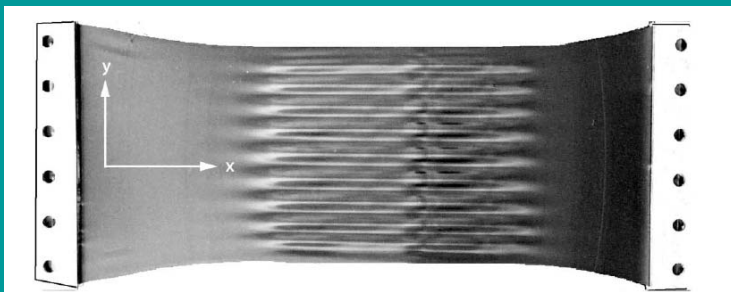
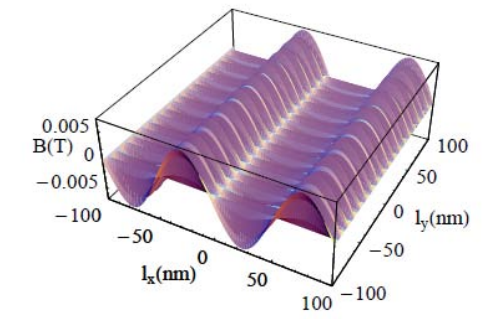
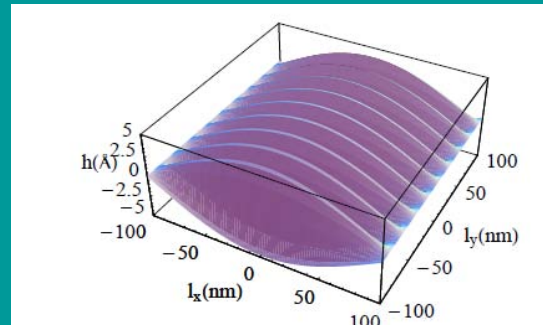
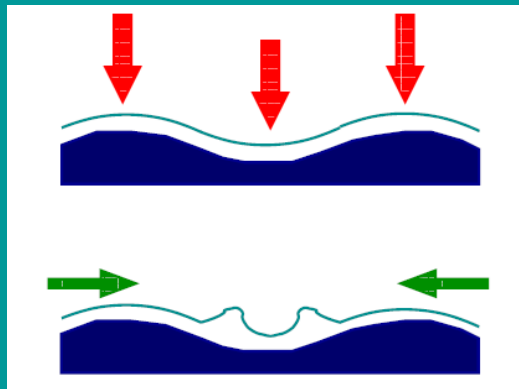


FIG. 1. Wrinkles in a polyethylene sheet of length $L \approx 25$ cm, width $W \approx 10$ cm, and thickness $t \approx 0.01$ cm under a uniaxial tensile strain $\gamma \approx 0.10$. (Figure courtesy of K. Ravi-Chandar)



E.Cerda and L. Mahadevan, Phys. Rev. Lett. **90**, 074302 (2003)



Possible instabilities in graphene on a substrate

Conclusions, open questions

- Fictitious gauge fields can be induced by strains, curvature, and topological defects
- Two non commuting gauge fields can be defined
- Height fluctuations can lead to significant fields.

$$\sigma = \frac{\partial \log(t)}{\partial \log(a)} \frac{h^2}{la} \approx 2 \frac{h^2}{la}$$

- Interaction effects may induce new phases at low carrier concentration.
- Strains and gauge fields will exist in suspended graphene samples under an applied field.
- The orbits in a real magnetic field are modified.
- “Dissipative” Quantum Hall physics may be induced

Midgap states and charge instabilities in corrugated graphene, F. G., M. I. Katsnelson, and M. A. H. Vozmediano, Phys. Rev. B 77, 075422 (2008)

Gauge field induced by ripples in graphene, F. G., B. Horovitz and P. Le Doussal, Phys. Rev. B 77, 205421 (2008)

Pseudomagnetic fields and ballistic transport in suspended graphene sheets, M. M. Fogler, F. G., and M. I. Katsnelson, Phys. Rev. Lett. **101**, 226804 (2008)

The electronic properties of graphene, A. H. Castro Neto, F. G., N. M. R. Peres,..A. K. Geim, K. S. Novoselov, Rev. Mod. Phys. **81**, 109 (2009)

M. A. H. Vozmediano, M. I. Katsnelson, F. G., to be published; A. K. Geim, M. I. Katsnelson, F. G., to be published